Available online at www.sciencedirect.com
SCIENCE DIRECT®
Journal of Magnetic Resonance 164 (2003) 256–269
JMR Journal of Magnetic Resonance
www.elsevier.com/locate/jmr

Evidence for a dipolar-coupled AM system in carnosine in human calf muscle from in vivo ^{1}H NMR spectroscopy

Leif Schröder* and Peter Bachert*

Biophysik und Medizinische Strahlenphysik, Deutsches Krebsforschungszentrum (dkfz), Im Neuenheimer Feld 280, D-69120 Heidelberg, Germany

Received 17 March 2003; revised 4 June 2003

Abstract

Spin systems with residual dipolar couplings such as creatine, taurine, and lactate in skeletal muscle tissue exhibit first-order spectra in in vivo ^{1}H NMR spectroscopy at 1.5 T because the coupled protons are represented by (nearly) symmetrized eigenfunctions. The imidazole ring protons (H2, H4) of carnosine are suspected to form also a coupled system. The ring's stiffness could enable a connectivity between these anisochronous protons with the consequence of second-order spectra at low field strength. Our purpose was to study whether this deviation from the Paschen–Back condition can be used to detect the H2–H4 coupling in localized 1D ^{1}H NMR spectra obtained at 1.5 T (64 MHz) from the human calf in a conventional whole-body scanner. As for the hydrogen hyperfine interaction, a Breit–Rabi equation was derived to describe the transition from Zeeman to Paschen–Back regime for two dipolar-coupled protons. The ratio of the measurable coupling strength (Sk) and the difference in resonance frequencies of the coupled spins ($\Delta\omega$) induces quantum-state mixing of various degree upon definition of an appropriate eigenbase of the coupled spin system. The corresponding Clebsch–Gordan coefficients manifest in characteristic energy corrections in the Breit–Rabi formula. These additional terms were used to define an asymmetry parameter of the line positions as a function of Sk and $\Delta\omega$. The observed frequency shifts of the resonances were found to be consistent with this parameter within the accuracy achievable in in vivo NMR spectroscopy. Thus it was possible to identify the origin of satellite peaks of H2, H4 and to describe this so far not investigated type of residual dipolar coupling in vivo.

Keywords: Carnosine; in vivo ^{1}H NMR; Human calf muscle; Second-order spectra; Breit–Rabi formula

1. Introduction

Recent in vivo ^{1}H NMR spectroscopy studies of human skeletal muscle suggest that the common model of a viscous liquid for the cytoplasm of living tissue, where molecular tumbling motion is isotropic and unrestricted, is inadequate for some "small" metabolites in striated muscle [1–3]. The spatial anisotropy of this structure seems to create conditions for a non-vanishing direct spin–spin coupling. This interaction can be quantified by the orientation-dependent line splitting $\Delta\nu(\theta)$ observed in ^{1}H NMR resonances of endogenous metabolites like creatine (Cr) and phosphocreatine (PCr):

$$\Delta\nu = \frac{3}{2} SD_0(3\cos^2\theta - 1), \tag{1}$$

where θ is the azimuthal angle of the internuclear vector with respect to the static magnetic field B_0. The order parameter S equals 1 for solids and 0 for isotropic liquids [4].

The residual dipolar couplings encountered in in vivo ^{1}H NMR so far involve first-order effects since the interactions concern isochronous spins or spins in different molecular groups with chemical shift differences that are large compared to the residual coupling strength SD_0. Examples for isochronous spin systems are the methylene groups of taurine (Tau), an A_2Z_2 system studied in [2], or the isolated methylene and methyl groups which constitute the A_2Z_3 system of (P)Cr [1,2,5]. In the AX_3 system of lactate (Lac) the residual coupling strength between methine and methyl protons is small compared to the chemical shift difference [3].

* Corresponding authors. Fax: +49-6221-422531.
E-mail addresses: l.schroeder@dkfz.de (L. Schröder), p.bachert@dkfz-heidelberg.de (P. Bachert).
URL: www.dkfz.de/mrspek. ">"

1090-7807/$ - see front matter © 2003 Elsevier Inc. All rights reserved.
doi:10.1016/S1090-7807(03)00205-2

The homonuclear residual dipolar couplings of spins in small molecules embedded in standard nematic phases are 10- to 10^3-fold stronger than scalar interactions [6], thus providing conditions close to the regime of the Zeeman effect at low field strengths (e.g., for dipolar-coupled AB systems at $B_0 = 1.5\,\mathrm{T}$, the standard field strength of whole-body MR tomographs). To identify second-order spectra at 1.5 T, the dipolar interaction strength must be comparable to J-couplings. In this case, the set of eigenfunctions of the coupled spin system is slightly changed and deviations from the normally valid Paschen–Back states are observed.

There are only a few metabolites detectable by in vivo NMR spectroscopy that exhibit resolved second-order spectra at 1.5 T: adenosine 5′-triphosphate (ATP) and citrate (Cit). To our knowledge, so far only the latter was studied concerning quantum-mechanical effects in the spectrum [7,8]. However, these phenomena are caused by scalar couplings and we will show that theory predicts a distinct behavior for dipolar-coupled spin systems.

In solid-state NMR where the direct spin–spin coupling is much stronger than the scalar interaction, it is difficult to observe second-order spectra at low field strengths ($B_0 = 1.5\,\mathrm{T}$), since the related effects, e.g., asymmetries in line intensities of spin multiplets, are strongly pronounced such that some satellites will be nearly invisible. However, if the dipolar coupling can be scaled down by molecular mobility to an interaction of low or intermediate strength, it could be possible to observe second-order spectra in low field.

This effect requires very specific conditions: on the one hand, the molecules must be highly mobile to reduce the coupling strength by several orders of magnitude. On the other hand, a certain degree of immobility is needed to prevent complete averaging of the dipolar coupling and to make the interaction strong enough to leave the Paschen–Back regime where first-order spectra are observed. We will demonstrate that this situation actually can occur in vivo.

The aromatic region of the in vivo ^{1}H NMR spectrum of the endogenous metabolite carnosine (Cs; β-alanyl-L-histidine) in muscle tissue shows orientation-dependent behaviour [9] as well as additional resonances [10]. The origin of this effect was not clearly identified, but dipolar coupling was a reasonable explanation. The major difference to the case of Cr and PCr is the involvement of a long-range coupling between two anisochronous spins: the Cs resonances detectable in vivo arise from the imidazole ring protons at positions 2 and 4 of the histidine residue. Their chemical shift difference is only 1 ppm, hence the coupling is not necessarily weak at 1.5 T. This could exclude a first-order spectrum.

2. Theory

Regarding dipolar couplings, NMR spectra of molecules in liquid phase and in most biological tissues in an external magnetic field B_0 are adequately described if rapid isotropic tumbling is assumed such that all terms of the Hamiltonian of the dipolar interaction of two spin-$\frac{1}{2}$ nuclei (I, S)

$$\hat{H}_{\mathrm{DD}} = \frac{\mu_0\hbar^2}{4\pi}\frac{\gamma_I\gamma_S}{r^3}(\hat{A} + \hat{B} + \hat{C} + \hat{D} + \hat{E} + \hat{F}) \tag{2}$$

average to zero. In the case of anisotropic motion, the secular part of the Hamiltonian, i.e., the operator $\hat{A} + \hat{B}$, yields a correct description of the spectra. This truncated operator can be transformed into

$$\hat{H}'_{\mathrm{DD}} = k\left(\hat{I}_z\hat{S}_z - \frac{1}{4}(\hat{I}_+\hat{S}_- + \hat{I}_-\hat{S}_+)\right), \tag{3}$$

where the flip-flop operators $\hat{I}_+\hat{S}_-$ and $\hat{I}_-\hat{S}_+$ are products of the rising and lowering operators $\hat{I}_\pm = \hat{I}_x \pm \mathrm{i}\hat{I}_y$, etc. and $k = (\mu_0\hbar^2/4\pi)(\gamma_I\gamma_S/r^3)(1 - 3\cos^2\theta)$ is the coupling constant. To describe systems which perform fast molecular tumbling motion, the effective coupling strength must include the order parameter, i.e., Sk. The only difference between the secular dipolar Hamiltonian in Eq. (3) and the operator $\hat{H}_J$ of scalar spin–spin coupling is the coefficient of the flip-flop operators: $-\frac{1}{4}$ in $\hat{H}'_{\mathrm{DD}}$ and $+\frac{1}{2}$ in $\hat{H}_J$. As a consequence, the principal-axis transformation of the Hamiltonian of dipolar coupling and calculated line positions and intensities are different from that of scalar-coupled spin systems.

The eigenfunctions of the Hamilton operator of Zeeman interaction and chemical shift are the four product states $\psi_1, \ldots, \psi_4$. Only two of these are also eigenfunctions of $\hat{H}'_{\mathrm{DD}}$, while $\psi_2 = |+-\rangle$ and $\psi_3 = |-+\rangle$ are inappropriate for the new eigenbase. A rotation in this Hilbert subspace generates two new eigenstates ψ'_2 and ψ'_3 of $\hat{H}'_{\mathrm{DD}}$. In the following we will apply the transformation matrix

$$\mathbf{U} = \begin{pmatrix} 1 & 0 & 0 & 0 \\ 0 & \cos\alpha & \sin\alpha & 0 \\ 0 & -\sin\alpha & \cos\alpha & 0 \\ 0 & 0 & 0 & 1 \end{pmatrix} \tag{4}$$

to the 4-dimensional eigenbase spanned by the initial product states. Orthonormality requires that the new eigenstates satisfy $\langle\psi'_2|H'_{\mathrm{DD}}|\psi'_3\rangle = 0$, which yields a relation for the rotational angle α, the coupling strength Sk, and the chemical shift $\Delta\omega = \omega_1 - \omega_2$ (assuming $\omega_1 > \omega_2$):

$$\frac{Sk}{2\hbar\Delta\omega} = \tan 2\alpha. \tag{5}$$

Thus angles in the range of $0° \leqslant \alpha \leqslant 45°$ are obtained in the case of dipolar interaction (and negative angles from the corresponding relation for J-coupled systems),

which is important for identification of the singlet state of the four eigenstates (see below). Principal-axis transformation of the Hamilton operator of Zeeman ($\mathbf{H}_Z$ in matrix representation) and dipolar interaction ($\mathbf{H}_{DD}$) with rotational angle α yields

$$\mathbf{H}_Z = \frac{\hbar}{2}\begin{pmatrix} -\omega_1-\omega_2 & 0 & 0 & 0 \\ 0 & -\Delta\omega\cos 2\alpha & 0 & 0 \\ 0 & 0 & \Delta\omega\cos 2\alpha & 0 \\ 0 & 0 & 0 & \omega_1+\omega_2 \end{pmatrix} \tag{6}$$

and

$$\mathbf{H}_{DD} = \mathbf{A} + \mathbf{B}(\alpha) \quad \text{with}$$

$$\mathbf{A} = \frac{Sk}{4}\begin{pmatrix} 1 & 0 & 0 & 0 \\ 0 & -1 & 0 & 0 \\ 0 & 0 & -1 & 0 \\ 0 & 0 & 0 & 1 \end{pmatrix},$$

$$\mathbf{B}(\alpha) = \frac{Sk}{4}\sin 2\alpha\begin{pmatrix} 0 & 0 & 0 & 0 \\ 0 & -1 & 0 & 0 \\ 0 & 0 & 1 & 0 \\ 0 & 0 & 0 & 0 \end{pmatrix}. \tag{7}$$

Accordingly, the new eigenstates $\{\psi_2', \psi_3'\}$ are degenerated with respect to operator $\hat{A}$. Because operator $\hat{B}$ induces the flip-flop transitions, it affects only the Hilbert subspace spanned by $\{\psi_2', \psi_3'\}$, thus generating two different quantum numbers for these two eigenstates.

As in the case of the hyperfine interaction of the hydrogen atom, we define the total spin operator $\hat{F} = \hat{S} + \hat{I}$ and obtain the set of operators $\{\hat{S}^2, \hat{I}^2, \hat{F}^2, \hat{F}_z\}$ which completely describes the coupled spin system for weak external fields. Breit and Rabi derived a formula for the corresponding quantum numbers that permits calculation of the energies of the states as a function of B_0 [11]. In particular it yields the energies in the range between the Zeeman and the Paschen–Back regime.

If the magnetic field increases, $\hat{F}$ is no more an adequate observable. The spin–spin coupling is broken up and the distinction between the singlet ($F = 0$) and the triplet state ($F = 1$) becomes obsolete. The appropriate operator to replace $\hat{F}$ is $\hat{B}$, because in high field the energy states of the spin system are classified according to the coupling strength. Nevertheless, m_F is still a good quantum number and appears in the Breit–Rabi formula.

By combining the Hamilton operators in Eqs. (6) and (7) we obtain the Breit–Rabi formula for a pair of dipolar-coupled protons. The energy of the states ψ_1 and ψ_4 depends linearly on B_0 owing to the term $\mp(\omega_1 + \omega_2)$ in $\mathbf{H}_Z$. Assuming that $\omega_1 + \omega_2 \approx 2\omega_0 = 2\gamma B_0$ we obtain

$$E_{1,4} = \frac{Sk}{4} \mp \hbar\gamma B_0. \tag{8}$$

Substitution of α by $\Delta\omega$ using Eq. (5) yields the energies of the other two levels, $E_{2,3}(B_0)$. The solution of the eigenvalue problem finally leads, with the relations $\sin(\arctan\alpha) = \alpha/\sqrt{1+\alpha^2}$ and $\cos(\arctan\alpha) = 1/\sqrt{1+\alpha^2}$ and the variable $x = 2\hbar\Delta\omega/Sk = 2\hbar\sigma\gamma B_0/Sk$, to the Breit–Rabi formula for two dipolar-coupled spin-$\frac{1}{2}$ nuclei:

$$E^{DD}(m_F, m_I, x) = Sk\left(\frac{(-1)^{1+m_F}}{4} - \frac{m_F}{2\sigma}x - \frac{(-1)^{-\frac{1}{2}+m_I}}{4}(1-|m_F|)\sqrt{x^2+1}\right). \tag{9}$$

The energies $E^{DD}(x)$ predicted by Eq. (9) are plotted in Fig. 1b. For comparison, Fig. 1a shows the Breit–Rabi diagram of the dipolar-coupled electron–proton spin system representing the hydrogen hyperfine interaction. Under conditions valid for the Paschen–Back effect (i.e., in the limit $B_0 \to \infty$), Eq. (9) transforms into

$$E^{DD}(m_F, m_I, x) = \frac{Sk}{4}(-1)^{1+m_F} - \left(\frac{m_F}{2\sigma} + \frac{(1-|m_F|)(-1)^{-\frac{1}{2}+m_I}}{4}\right)Skx,$$

which predicts a linear relationship between E^{DD} and B_0 in high field. The corresponding asymptotic lines are also drawn in Fig. 1b.

The transformation, Eq. (4), with its Clebsch–Gordan coefficients $\cos\alpha$ and $\pm\sin\alpha$ induces changes in line positions, intensities, and phase modulations that differ from that of the simple AX system. They will be discussed now successively to exploit them for evaluating the experimental results.

2.1. Line positions

According to Eq. (9) the line positions depend on the coupling strength. The four detectable single-quantum coherences produce two doublets centred at ω_1 and ω_2, respectively. For example, the energies of the transitions $1 \leftrightarrow 3$ and $2 \leftrightarrow 4$ are

$$E_{13} = \hbar\omega_1 - \frac{Sk}{2} - \hbar\Delta\omega\sin^2\alpha + \frac{Sk}{2}\sin\alpha\cos\alpha, \tag{10}$$

$$E_{24} = \hbar\omega_1 + \frac{Sk}{2} - \hbar\Delta\omega\sin^2\alpha + \frac{Sk}{2}\sin\alpha\cos\alpha. \tag{11}$$

Both resonances are shifted in frequency by the same amount, hence the line splitting is $\Delta\nu = (E_{24} - E_{13})/h = Sk/h = \text{constant}$. Eqs. (10) and (11) demonstrate a characteristic property of second-order spectra: The line splitting is asymmetric with respect to the primary line position $\hbar\omega_1$. One doublet is the mirror-image of the other, hence an asymmetry parameter can be defined:

$$A_P(\alpha, \Delta\omega) = -\hbar\Delta\omega\sin^2\alpha + \frac{Sk}{2}\sin\alpha\cos\alpha,$$

or, using Eq. (5),

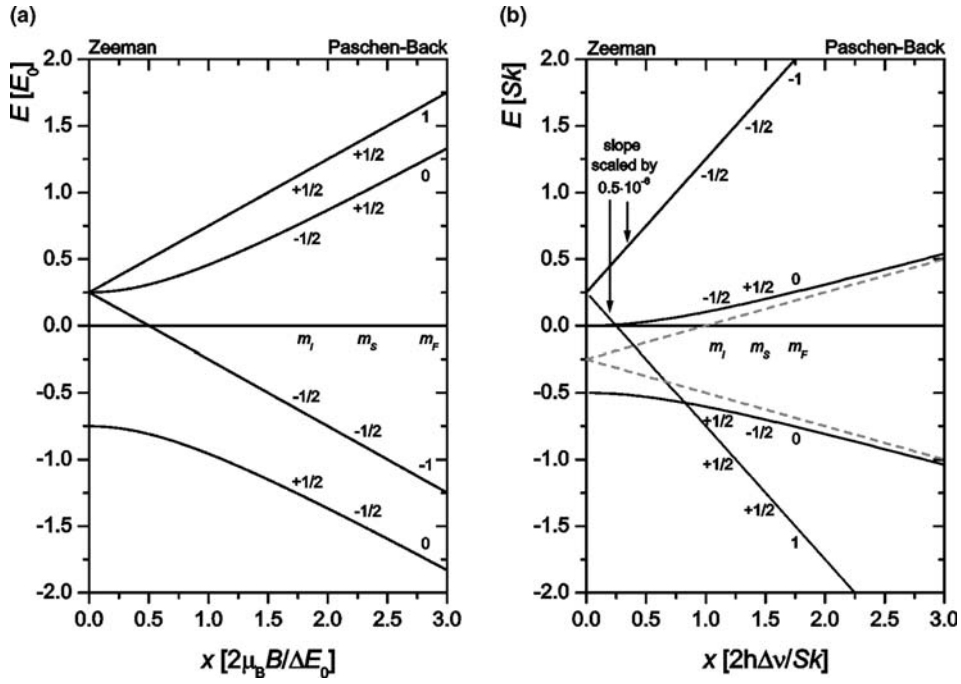

Fig. 1. Breit–Rabi diagram for the electron–proton hyperfine interaction in the hydrogen atom (a) and for a system of two dipolar-coupled anisochronous protons (b). The values of the quantum numbers m_I, m_S, and m_F are indicated; in (b) the slope of the two linear branches is scaled down by a factor of 0.5×10^{-6} for illustration.

$$A_{\mathrm{P}}(\alpha) = Sk\left(\frac{\sin 2\alpha}{4} - \frac{\sin^2 \alpha}{2\tan 2\alpha}\right). \tag{12}$$

2.2. Relative signal intensities

Another important property of second-order spectra is the inequality of multiplet intensities. Since always one state vector of the tilted two-dimensional subbase $\{\psi'_2, \psi'_3\}$ is involved in single-quantum coherences, the line intensities depend on the rotational angle α. This effect reflects the forbidden intercombination between singlet and triplet states when the coupling strength increases. Since α is positive in the case of dipolar coupling, the triplet state derives from ψ_3 of the AX system and, accordingly, the two inner resonances of the two doublets show reduced intensities (Fig. 2). This is in contrast to the "roof effect" of scalar coupling which is characterised by lower intensities of the outer satellites.

The probabilities of transitions between states ψ_j and ψ_i are obtained with Fermi's golden rule involving the Hamilton operator $\hat{H}_{\mathrm{RF}}(t)$ which describes the effect of the applied radiofrequency field. To simplify the calculation, we employ

$$\langle\psi_i|\hat{H}_{\mathrm{RF}}(t)|\psi_j\rangle = \frac{1}{2}\langle\psi_i|\left(\omega_1\left(\hat{I}_+ + \hat{I}_-\right) + \omega_2\left(\hat{S}_+ + \hat{S}_-\right)\right)|\psi_j\rangle. \tag{13}$$

For isochronous spins, $\omega_1 = \omega_2 \Rightarrow \alpha = 45°$ (Eq. (5)), the coupling can be treated as a very strong interaction. Thus $\hat{H}_{\mathrm{RF}}(t)$ applied to ψ'_3 yields $\hat{H}_{\mathrm{RF}}(t)|\psi'_3\rangle = 0$ and Eq. (13) excludes intercombination completely. As a consequence, only two single-quantum coherences remain and Eq. (11) and its analogue for the transition $1 \leftrightarrow 2$ read

$$E_{12} = \hbar\omega_0 + \frac{3Sk}{4} \quad \text{and} \quad E_{24} = \hbar\omega_0 - \frac{3Sk}{4}. \tag{14}$$

Accordingly the line splitting for isochronous coupling, as observed for Cr and PCr in muscle tissue in vivo, is larger by a factor of 1.5 ($\Delta\nu_{\mathrm{iso}} = 1.5\Delta\nu$), and the

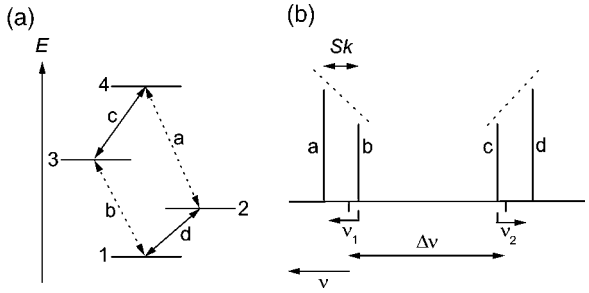

Fig. 2. The effects of increasing quantum state mixing on spectra of dipolar-coupled two-spin systems. (a) Energy levels and observable transitions. The energy level belonging to the singlet state (for strong coupling) is shown in grey. (b) Corresponding spectrum illustrating the inequality (dashed lines) of line intensities owing to forbidden intercombination. The changes in line positions are indicated by bent arrows: Doublet (a, b) is shifted downfield, doublet (c, d) upfield.

spectral pattern becomes symmetric as in the case of first-order spectra. Coupling constants must be indicated carefully: The dependency of dipolar line splitting on spatial orientation including the factor 1.5 can be applied to A_2 systems like (P)Cr and Tau. In contrast, the connectivities studied in [3] represent an AX_3 system and the reported dipolar line splitting of $Sk/h \approx 24$ Hz (including the scalar coupling of 7 Hz) should be quantified rather by a coupling constant $SD_0 \approx -8.85$ Hz than by $SD_0 \approx -5.9$ Hz.

For $\alpha < 45°$, i.e., coupling of anisochronous spins, theory predicts four single-quantum transitions. For homonuclear coupling $\omega_2 = \omega_1 - \Delta\omega \approx \omega_1$ (referring to [12]) we obtain the line intensities for the doublet with the transition energies of Eqs. (10) and (11):

$$I_{13} \propto 1 - \sin 2\alpha \quad \text{and} \quad I_{24} \propto 1 + \sin 2\alpha. \tag{15}$$

The ratio I_{13}/I_{24} can be considered as asymmetry parameter A_I for the intensities. Like $A_P(\alpha)$, Eq. (12), A_I depends only on α. However, the line intensities are modified by phase modulation in multi-pulse experiments.

2.3. Phase modulations

The ^{1}H NMR signals of strongly scalar-coupled spin systems are affected by complex phase modulation occurring during STEAM or PRESS localization sequences [8,13]. As a consequence of the connectivities between the resonances established by the inversion pulse of the spin-echo experiment, the outer signals (a and d, Fig. 2) are modulated faster than the inner ones (b and c, Fig. 2). The result is the same for scalar- and dipolar-coupled spin systems [14]. However, the faster modulation of the initially intense resonances a and d could invert the roof effect of dipolar interaction resembling that of J-coupling. This means that the effect cannot be used directly to identify connectivities as in the case of 1D spectra of scalar-coupled systems. Moreover, the asymmetry parameter A_I is inappropriate to evaluate the coupling strength.

Altogether, theory gives the following predictions: A system of protons with residual dipolar couplings exhibits spectra that permit the identification of connectivities not only by means of the line splitting $\Delta\nu$ from Eq. (1), but also by subtle quantum mechanical effects. The asymmetry parameter A_P must also be taken into account and it has to be consistent with the observed $\Delta\nu$ because both quantities are connected through the Breit–Rabi parameter x. Without application of advanced operator formalism, effects like altered line intensities and the related phase modulations can be used only for a qualitative analysis of localized in vivo ^{1}H NMR spectra.

The same transformation which leads to the Breit–Rabi formula (Eq. (9)) yields A_P as a function of x (which is the more convenient variable, since it contains the parameters $\Delta\omega$ and Sk which can be derived directly from in vivo spectra):

$$A_P(x) = \frac{Sk}{2}\left(\frac{1}{2}\sin\arctan\left(x^{-1}\right) - x\sin^2\frac{\arctan\left(x^{-1}\right)}{2}\right). \tag{16}$$

Since A_P is positive, the doublet with the transitions $1 \leftrightarrow 3$ and $2 \leftrightarrow 4$ is shifted downfield as in the case of a scalar-coupled system. The plot in Fig. 3 shows that the asymmetry parameter does not change significantly for $x > 1$, thus strong couplings where $x \simeq 1$, i.e., $Sk/\hbar\Delta\omega \approx 2$, are interesting. However, intercombination is nearly completely forbidden in this case. As a consequence, the smaller resonances b and c in the case of strong interactions will be difficult to resolve and a symmetric spectrum will arise comprising only the signals a and d. This explains why the dipolar coupling in nematic phases ($Sk/h \approx 10^2$–10^4 Hz) could complicate the identification of four resonances at 1.5 T.

This is different in the case of tissue metabolites with restricted mobility ($Sk/h \approx 10$ Hz). Because x is still in the order of 1 these spin systems are subject to an intermediate between Zeeman and Paschen–Back condition. Thus all four resonances as well as a slight asymmetry of the line positions are detectable. For very weak couplings the asymmetry will disappear because of $x \to \infty$ and genuine first-order spectra are observed.

Because of the remaining high molecular mobility in vivo it is reasonable to assume that $\hbar\Delta\omega > Sk$ for Cs ($\Delta\omega \approx 1$ ppm). Hence, the parameter x will never be smaller than 2, which is the regime described above: A_P

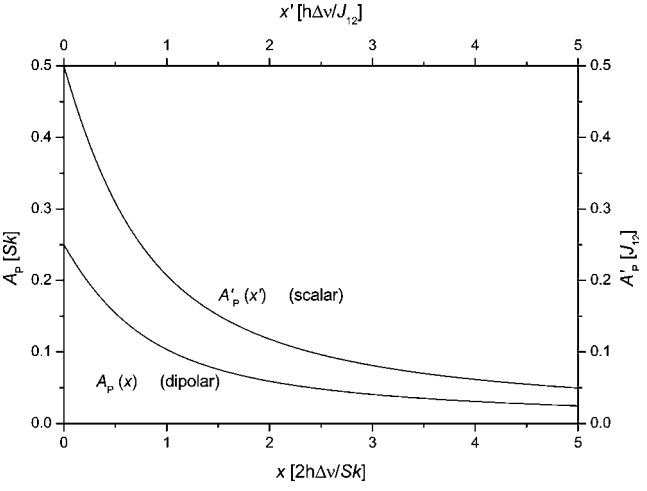

Fig. 3. Asymmetry parameter A_P of transitions a and b (Fig. 2) for a dipolar-coupled pair of spins as a function of the coupling strength, in terms of the Breit–Rabi parameter x (Eq. (16)). The analogous shift $A'_P(x')$ for a J-coupled system is shown for comparison (theory not presented in this contribution). Since both quantities are positive, the doublet a, b is shifted down-field in each case and the nature of the coupling manifests only in the magnitude of A_P.

does not depend significantly on x, but the aberrations from the Paschen–Back condition are already detectable. The values for α together with Eq. (15) predict two doublets. Accordingly for dipolar AM systems in vivo we expect a spectrum with four resolved signals and a small asymmetry in line positions.

3. Experimental

Proton NMR experiments were performed at $B_0 = 1.5\,\mathrm{T}$ on a whole-body tomograph (MAGNETOM Vision Plus; Siemens AG, Erlangen, Germany) equipped with a highly homogeneous magnet (HELICON model 2E; Siemens). In experiments on model solutions the standard head coil was used for RF excitation and detection. In vivo examinations were performed on the leg of volunteers in supine position using the body resonator for RF excitation and and a standard flex extremity coil ($17 \times 37\,\mathrm{cm}^2$) for signal detection.

3.1. ^1H NMR spectroscopy of model solutions

Model solutions of 50 mM carnosine (Sigma–Aldrich Chemie GmbH, Steinheim, Germany) were prepared (physiological pH with 0.1 M HCl buffer) to obtain spectra from samples which do not exhibit residual dipolar couplings. Localized shim resulted in water proton line widths (FWHM) of $\Delta\nu_{1/2} = 3$–$4\,\mathrm{Hz}$ for a 8-ml voxel. Localized spectra were obtained with the STEAM sequence (stimulated echo acquisition mode) with a single 25.6-ms frequency-selective Gaussian-shaped RF pulse for water-signal suppression and the measurement parameters: repetition time $TR = 2\,\mathrm{s}$, echo delay $TE =$ 10 ms, middle interval $TM = 15\,\mathrm{ms}$, number of excitations $NEX = 256$, voxel size $= (2\,\mathrm{cm})^3$. To detect signal modulations owing to possible scalar coupling between the two imidazole ring protons the same sequence was applied with variable TE in the range of 135–270 ms ($TR = 1.5\,\mathrm{s}$).

3.2. In vivo ^1H NMR spectroscopy

Localized ^{1}H NMR spectra were obtained from two different muscles of the right leg of healthy male volunteers ($n = 5$). Informed consent was obtained from all volunteers prior to the NMR examination. After acquisition of MR images in three orthogonal slices, voxels of $(2\,\mathrm{cm})^3$ were placed in m. gastrocnemius and m. soleus. Shim in the voxel produced a minimum line width of $\Delta\nu_{1/2} = 18\,\mathrm{Hz}$ of the tissue water proton resonance. The pennation angle, i.e., the fibre orientation with respect to B_0, of m. gastrocnemius within the voxel was estimated by means of the dipolar line splitting of the (P)Cr methylene resonance using Eq. (1) with $SD_0 = 4.92\,\mathrm{Hz}$ from [1] (an Euler transformation can be neglected).

The STEAM sequence was applied with two 25.6-ms chemical-shift-selective Gaussian-shaped RF pulses at around $\delta = 4.7$ and 1.4 ppm for water- and lipid-signal suppression, respectively, and the measurement parameters: $TR = 2\,\mathrm{s}$, $TE = 10\,\mathrm{ms}$ (minimum), $TM = 15\,\mathrm{ms}$, $NEX = 500$, acquisition time $AQ = 1024\,\mathrm{ms}$, voxel size $= (2\,\mathrm{cm})^3$. The volunteers were able to keep the leg motionless during the measurement time of 16.8 min.

3.3. Data processing and analysis

FIDs were processed using a commercial program (LUISE; Siemens) available at the MAGNETOM Vision scanner. After zero-filling to 4096 complex data points which yields 0.004 ppm (0.25 Hz) spectral resolution, signal-time data were multiplied by a Gaussian function (time constant, 200 ms.) for line broadening, followed by Fourier transformation, phase and baseline correction. The Fourier spectra were analyzed by means of the LUISE least-squares fit routine assuming Gaussian lineshapes of the resonances. Chemical shift values are given in ppm relative to the standard reference tetramethylsilane (TMS) at $\delta = 0.0$ ppm. Data were displayed using Origin® 6.1 (OriginLab, Northampton, MA, USA) and chemical structures were drawn using the software ISIS/Draw 2.3 (MDL Information Systems, San Leandro, CA, USA) and ACD/3D 4.52 (Advanced Chemistry Development, Toronto, Canada).

4. Results

In ^{1}H NMR spectra of carnosine in aqueous solution at pH 7.08 two aromatic resonances could be resolved at $\delta = 7.02$ and 7.96 ppm (Fig. 4) and assigned to the imidazole ring protons H2 and H4 according to [15]. Chemical shifts of these peaks depend on solvent pH. The chosen pH corresponds to the physiological value of pH 7.07 ± 0.02 of human skeletal muscle which we measured in a former in vivo ^{31}P-{^{1}H} NMR spectroscopy study on the calf of volunteers ($n = 17$, age: 21–34 yr). Fit of Gaussian line shapes to the observed peaks yields equal intensities (within error limits of fit routine) of H2 and H4 resonances. This corresponds to expectation.

The analysis of a series of spectra of the Cs model solution obtained with echo delays in the range of $TE = 135$–$265\,\mathrm{ms}$ (increment: $\Delta TE = 10\,\mathrm{ms}$) showed only a monotonous decrease of the signal without modulation (data not shown). This excludes a significant scalar coupling of the two imidazole ring protons.

Aliphatic signals assigned to the methylene groups of histidine and β-alanine and the signal of the histidinyl α-CH proton resonate between $\delta = 2.5$ and 4.4 ppm (Fig. 4). Spectral resolution at 1.5 T was insufficient to detect all scalar line splittings, but peak assignment was

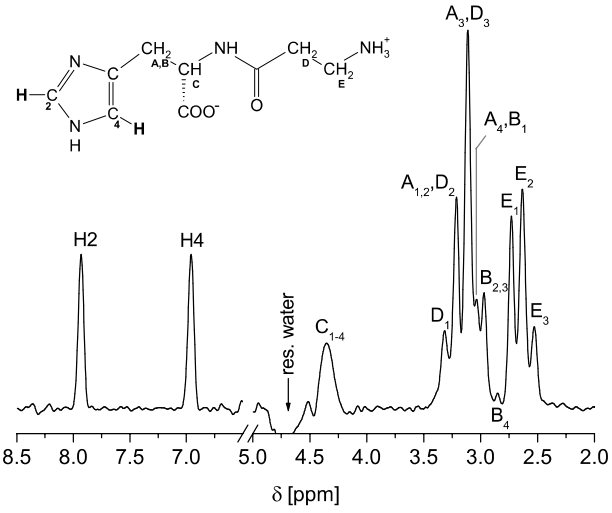

Fig. 4. Chemical structure of the endogenous dipeptide carnosine (Cs) and 1.5-T ^{1}H NMR spectrum of a 50-mM model solution of Cs. Besides the imidazole ring proton resonances H2 and H4 aliphatic multiplets appear at chemical shifts between $\delta = 2.5$ and 4.4 ppm. Two triplets ($D_{1–3}$, $E_{1–3}$) are assigned to the methylene protons of the β-alanyl residue, the D triplet overlaps with the 8 resonances of the histidine methylene signals ($A_{1–4}$, $B_{1–4}$). The four resonances of proton C could not be resolved (STEAM with water-signal suppression; measurement parameters $TR = 2$ s, $TE = 10$ ms, $TM = 15$ ms, $NEX = 256$, voxel size = (2 cm)^3).

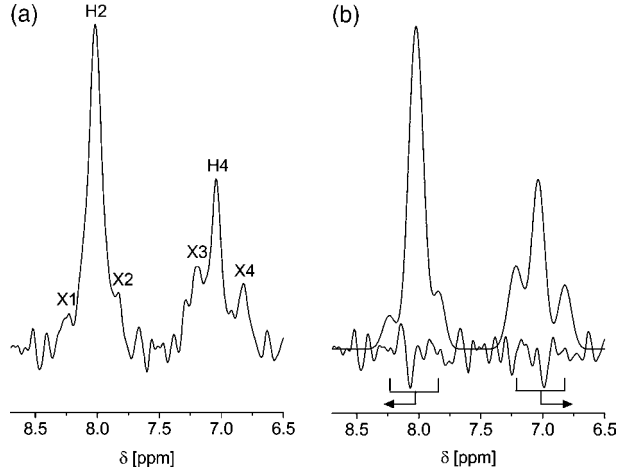

Fig. 5. Aromatic region with carnosine resonances of a localized in vivo 1.5-T ^{1}H NMR spectrum of m. gastrocnemius of a volunteer (a). In addition to the imidazole ring proton signals at $\delta \approx 7$ ppm (H4) and 8 ppm (H2), four satellite peaks (X1–X4) are resolved. Fitted spectrum assuming Gaussian line shapes and the residual signal after subtraction of the fit curve from the measured data (b). Subsuming X1 and X2 as well as X3 and X4 into doublets, these are shifted relative to H2 and H4, respectively (arrows). (STEAM with water- and lipid-signal suppression; $TR = 2$ s, $TE = 20$ ms, $TM = 15$ ms, $NEX = 500$, voxel size = (2 cm)^3).

possible by comparing data to previously published Cs spectra [16]. The β-alanine-methylene groups form a scalar-coupled spin system which exhibits a second-order spectrum. The resulting asymmetries of signal intensities are visible only for the triplet $E_{1–3}$; the other triplet ($D_{1–3}$) overlaps with the resonances from proton A. The coupling ($J \approx 6.3$ Hz) appears like a relatively strong interaction, because the chemical-shift difference of the triplets is only 0.59 ppm (≈ 37 Hz at 1.5 T).

Localized short-TE in vivo ^{1}H NMR spectra from m. gastrocnemius showed not only the two resonances at $\delta = 7$ and 8 ppm of Cs imidazole ring protons [17]. In addition, up to four resonances (X1–X4), two satellites at each main signal, could be detected in the aromatic region (Fig. 5). Because of the larger intensity and line width of the H2 resonance, it was sometimes easier to resolve X3 from H4 than X2 from H2. The significant discrepancy between the intensities of H2 and H4 in vivo was previously reported by other groups [9,18].

Fig. 6 shows the Cs spectral region of in vivo ^{1}H NMR spectra obtained with $TE = 10, 20, 30$, and 40 ms from m. gastrocnemius. T_2 relaxation of H4 protons seems to be faster than that of H2. The data indicate $TE \leqslant 20$ ms for appropriate detection of X1–X4. Moreover, inspection of Figs. 5 and 6 shows an asymmetry of the positions of these peaks which is well-known for second-order spectra: X2 and X3 are closer to the central lines than the outer satellites X1 and X4. The centre of the supposed doublet near 7 ppm is shifted to lower,

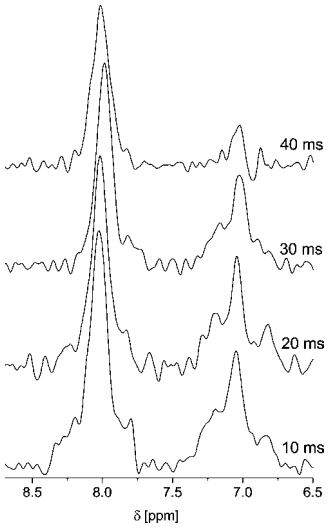

Fig. 6. Carnosine region of localized in vivo 1.5-T ^{1}H NMR spectra obtained with $TE = 10$, 20, 30, and 40 ms from m. gastrocnemius of a volunteer (STEAM with water- and lipid-signal suppression; $TR = 2$ s, $TM = 15$ ms, $NEX = 500$, voxel size = (2 cm)^3).

the other (X1, X2) near 8 ppm to higher frequencies. The four satellites could not be resolved in all experiments (10 spectra altogether) we performed, but the line shapes always indicated that the signal originates from more than two single resonances.

A fit of the recorded spectra was possible in five studies, the resulting data are found in Tables 1 and 2

Table 1
Chemical shifts of aromatic resonances detected in the carnosine spectral region of localized in vivo ^{1}H NMR spectra of m. gastrocnemius of $n = 5$ volunteers (chemical shift reference: TMS, $\delta = 0.0$ ppm)

Study #	δ X1 (ppm)	δ H2 (ppm)	δ X2 (ppm)	δ X3 (ppm)	δ H4 (ppm)	δ X4 (ppm)	$\Delta\nu_{1,2}$ (ppm)	$\Delta\nu_{3,4}$ (ppm)	θ (°)
1	8.235	8.023	7.837	7.220	7.040	6.832	0.40	0.39	27.0
2	8.210	7.945	7.720	7.190	6.985	6.720	0.49	0.47	14.4
3	8.410	8.060	7.830	7.325	7.100	6.815	0.58	0.51	8.3
4	—	8.020	7.820	7.370	7.120	6.825	—	0.55	0.0
5	8.250	8.005	7.780	7.270	7.060	6.830	0.47	0.44	20.7

The spectral resolution after zero-filling is 0.004 ppm and the evaluation software (LUISE) yields three digits for line positions; all values are rounded to 0.01 ppm. $\Delta\nu_{1,2}$ and $\Delta\nu_{3,4}$ are the line splittings of X1, X2 and X3, X4 doublets, respectively. θ is the angle between muscle fibre axis and the direction of the static magnetic field B_0 (''pennation angle'') derived from the splitting of the (P)Cr CH_2 doublet with use of Eq. (1).

Table 2
Asymmetry parameters of line positions of (X1, X2) and (X3, X4) doublets relative to the central resonances assigned to H2 and H4 protons of carnosine of localized in vivo ^{1}H NMR spectra from m. gastrocnemius

Study #	Shift 1,2 (ppm)	Shift 3,4 (ppm)	Sk/h (ppm)	x ($2h\Delta\nu/Sk$)	Expected A_P (Sk)	Expected A_P (ppm)
1	+0.01	−0.01	0.40	5.00	±0.025	±0.01
2	+0.02	−0.03	0.48	4.00	±0.031	±0.02
3	+0.06	−0.03	0.55	3.52	±0.035	±0.02
4	—	−0.02	0.55	3.30	±0.037	±0.02
5	+0.01	−0.01	0.46	4.15	±0.030	±0.01

(X1 could not be resolved in study #4). Table 1 gives chemical shifts and the pennation angle θ (muscle fibre orientation with respect to B_0) calculated from the line splitting of the (P)Cr methylene doublet using Eq. (1) (see methods). For study #4 the observed splitting of 15.5 Hz was slightly larger than the maximum reported in [1]. In this case θ was not defined by Eq. (1) and we assume a pennation angle of 0°. The accuracy of the evaluated line splittings is 0.7 Hz. This results in large uncertainties for small values of θ (±5.0° for study #4) and smaller ones for larger pennation angles (±1.2° for study #1).

The chemical-shift differences $\Delta\nu_{1,2}$ and $\Delta\nu_{3,4}$ of (X1, X2) and (X3, X4), respectively, are very similar. Their average is a measure of the coupling constant introduced in Eq. (3): $(\Delta\nu_{1,2} + \Delta\nu_{3,4})/2 = (Sk/h)$. Table 2 gives the values of this quantity together with the Breit–Rabi parameter x (with $\Delta\omega \simeq 1$ ppm as chemical shift difference of the central peaks), the corresponding asymmetry parameter $A_P(x)$ (Eq. (16)), and the measured upfield and downfield shifts (difference of centre peak position and mean of satellite frequencies). An accurate evaluation of the intensities of the satellite peaks was not possible due to low S/N.

The aliphatic region of water- and fat-signal-suppressed in vivo ^{1}H NMR spectra of m. gastrocnemius shows resonances of creatine and phosphocreatine ((P)Cr) and of compounds (mainly cholines, Cho) with a trimethylamine (TMA) group (Fig. 7). The residual dipolar coupling of (P)Cr causes a pronounced line splitting of the methylene (doublet centred at $\delta = 3.93$ ppm) and the methyl proton resonance (triplet, $\delta = 3.03$ ppm). This effect was first reported by Kreis and Boesch [1,19]. Indications of dipolar couplings which also affect the resonances of Tau in this muscle can be infered from the observed downfield shift of this signal. The resonances of the N–CH_2 ($\delta = 3.25$ ppm) and the S–CH_2 group ($\delta = 3.42$ ppm) are expected to yield only one broad signal at ca. 3.34 ppm at 1.5 T

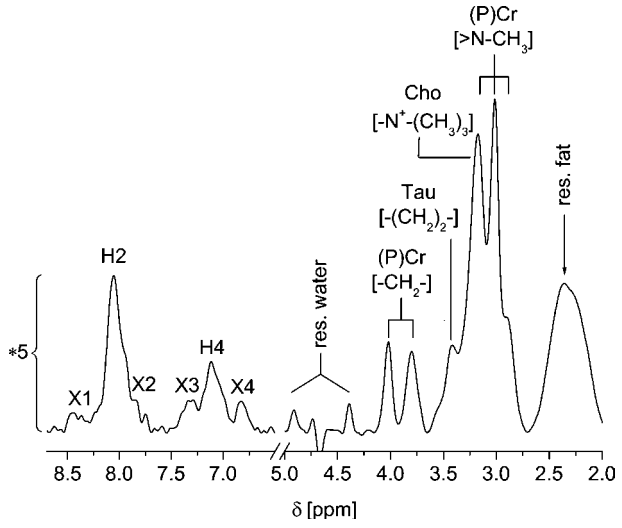

Fig. 7. Localized in vivo 1.5-T ^{1}H NMR spectrum from m. gastrocnemius of a volunteer. The intensities of the aromatic region are magnified by a factor of 5 to display the four satellites (X1–X4) of imidazole ring proton resonances (H2, H4). Residual dipolar coupling affects several resonances in the aliphatic region of the spectrum: the methylene and methyl multiplets of (P)Cr, the latter partly overlap with the choline signal (Cho); the taurine (Tau) signal is shifted downfield. No aliphatic resonances of Cs are detectable (STEAM with water- and lipid-signal suppression; $TR = 2$ s, $TE = 17$ ms, $TM = 15$ ms, $NEX = 500$, voxel size = $(2\,\text{cm})^3$).

because of second-order effects. This peak seems to be split up into two signals; one of them resonates at $\delta = 3.42$ ppm. Because of the intense signal of TMA it is not possible to resolve the other part of the doublet caused by residual dipolar coupling [2].

In distinct contrast to m. gastrocnemius, in m. soleus the residual dipolar coupling of (P)Cr nearly vanishes as reported previously [1]. Only two broad signals are visible at $\delta = 3.93$ ppm and 3.03 ppm (Fig. 8). One signal from both methylene groups in Tau appears at $\delta = 3.34$ ppm at the downfield shoulder of the TMA signals. No aliphatic resonances of Cs can be detected. The signal at $\delta = 3.66$ ppm (Fig. 8) could not be identified. The assignment to $>N–CH_3$ protons of anserine (their signal is pH-dependent and resonates between $\delta = 3.84$ and 3.62 ppm in model solution, [15]) is inadequate since human skeletal muscle contains almost no anserine [20]. In spectra of m. gastrocnemius this peak might be superimposed by the close (P)Cr doublet. The strong attenuation of residual dipolar couplings in m. soleus also simplifies the spectra at the low-field side of the water resonance ($\delta > 4.7$ ppm), as displayed in Fig. 8. The X2 and X3 satellites coincide with the centre peaks, the X1 and X4 resonances move closer to them, and the difference of H2 and H4 signal intensities decreases.

Compared to the spectrum in Fig. 7, the overall Cs signal intensity is lower. This agrees with the known fact that Cs is essential for pH buffering in glycolysis [21] which occurs at a higher rate in m. gastrocnemius than in m. soleus.

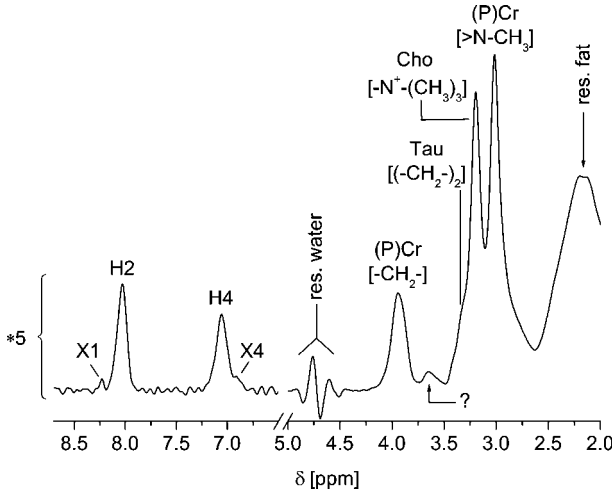

Fig. 8. Localized in vivo 1.5-T ^{1}H NMR spectrum from m. soleus of a volunteer. The intensities of the aromatic region are magnified by a factor of 5. Only the outer satellites X1 and X4 (now closer to the centre peaks) can be resolved and the intensity of the H4 imidazole ring proton approaches that of H2. (P)Cr signals appear as single broad resonances indicating attenuated dipolar couplings compared to the situation in m. gastrocnemius. The taurine signal (from $>N–CH_2–$ and $–CH_2–SO_3^-$) is not shifted as in the spectrum in Fig. 7. The signal at $\delta = 3.66$ ppm could not be assigned. No aliphatic resonances of Cs are detectable (STEAM with water- and lipid-signal suppression; $TR = 2$ s, $TE = 17$ ms, $TM = 15$ ms, $NEX = 500$, voxel size $= (2\,\text{cm})^3$).

5. Discussion

The observed discrepancy between ^{1}H NMR spectra of Cs in model solution and in intact human m. gastrocnemius is remarkable. A spectrum of aromatic Cs resonances obtained from human forearm muscle with additional, asymmetric signals has already been published [18], but was not analyzed in this respect.

A recent study [22] reported additional peaks at the downfield side of the aromatic Cs resonances owing to variable acidity of different types of muscle fibres upon contraction. This phenomenon can be excluded in our case, since first we obtained spectra from resting muscle where pH will be constant, and, secondly, we observed satellites up- and downfield from the H2 and H4 signals, while with decreasing pH additional peaks were seen only at the downfield side [22].

Previous in vivo studies demonstrated that anisotropic muscle-fibre structures can affect the ^{1}H NMR resonances of (P)Cr [1,5,19,23], Tau [2], and Lac [3]. These orientation-dependent effects were attributed to residual dipolar couplings. Since magnetic susceptibility variations within the tissue could be excluded as an explanation [3,19], it therefore appears that a pool of Cs molecules with restricted mobility exists in skeletal muscle tissue which causes the satellite lines by virtue of a non-vanishing dipolar coupling. The resonances at 7 and 8 ppm are generated by the pool of freely tumbling Cs molecules. Likewise, two pools—one where scalar and dipolar, the other where only scalar coupling is effective—were proposed for Lac and attributed to intracellular and extracellular compartments [3]. In contrast, Cs is entirely intracellular; it is a large and charged molecule with neglegibile permeability to the cell membrane. It can be speculated that for the total intracellular volume there is a difference between the mobility of Cs in the myofibrillar space and elsewhere in the cytoplasm.

Unfortunately the fast T_2 relaxation [17] (e.g., the H4-signal vanishes nearly after 40 ms, Fig. 6) prevents the observation of possible couplings in the aromatic region via phase modulation. Likewise, 2D experiments are inappropriate since the measurement time is too long for examination of humans. Hence data from previous studies in combination with our theoretical model must be employed.

Several proton–proton interactions within the molecule can cause the observed line splitting. Alonso et al. [24,25] detected cross peaks in two-dimensional spectra of Cs ex vivo indicating a correlation between H2 and H4. Interestingly they also observed a scalar interaction in model solution [24]. But the coupling constant must be smaller than 2 Hz since at this resolution couplings

could be resolved only within the aliphatic region [16]. In agreement with the missing signal modulation in our experiments a significant scalar coupling of H2–H4 can therefore be excluded. Moreover, J-coupling of the two ring protons with the adjacent NH group can be neglected since this proton undergoes fast chemical exchange and will be undetectable ([26] quotes $J \approx 1$ Hz for this system). Altogether, J-couplings cannot explain the resonances X1–X4 in localized ^{1}H NMR spectra of m. gastrocnemius.

Spectra of excised intact frog gastrocnemius muscle tissue showed additional cross peaks in homonuclear Hartmann–Hahn (HOHAHA) experiments when compared to spectra of muscle extracts or model solution [25]. The only explanation for these peaks was rotating-frame Overhauser enhancement (ROE), the corresponding connectivities are displayed in Table 3. ROE peak #4 results from the scalar coupling ($J \approx 6.3$ Hz) between protons D and E combined with ROE peak #3. Both were assigned to the NH group of the imidazole ring (which normally cannot be detected). Besides the interaction between H4 and the histidinyl β-CH_2 protons (A, B), there is also a direct coupling between the two ring protons H4 and H2.

Only in the case of long correlation times τ_c ROE peaks have the same intensities as HOHAHA coherence transfer peaks. For this reason, the tumbling of Cs in vivo must be restricted (a binding of Cs with a protein on the myofibril is proposed in [25]). Therefore, line splitting or broadening might also be detectable in 1D spectra.

This way the analysis of ROE peaks can help to explain the observed satellites of Cs resonances. The downfield shift of the supposed doublet X1, X2 relative to H2 suggests a connectivity of the resonance at $\delta = 8$ ppm with a resonance at the high-field side in agreement with the observed ROE peak #1. In this case the satellites X1, X2 will result from an interaction between H2 and H4—an argument which is also supported by the similar line splittings $\Delta\nu_{1,2}$ and $\Delta\nu_{3,4}$ (Table 1) and the complementary upfield shift of X3 and X4. Yet the observed discrepancy of the intensities of H2 and H4 remains to be explained. ROE peaks #3 and #4 are informative in this respect since they indicate that the amino proton of the histidine ring of Cs in intact m. gastrocnemius will not undergo fast exchange. Hence, an additional signal is expected in vivo.

Arús and Bárány [15] first assigned a signal close to the H2 resonance to the amide proton of the Cs peptide group and later attributed ROE peaks #3 and #4 at $\delta = 8$ ppm to connectivities between the alanyl-CH_2 groups and the NH proton of the imidazole ring (Table 3). But the internuclear distance of the latter is large, hence we rather assume that the proton of the closer peptide group is the origin of ROE peaks #3 and #4. The signal of the similar NH group in N-acetylaspartate (NAA) is a broad doublet with $J = 6.4$ Hz in vivo [26].

Presently, the problem of the NH groups of Cs is not completely resolved, we can only conclude: One of the NH protons is involved in Cs binding to some unknown structure (e.g., by hydrogen-bond formation with a macromolecule) and yields a signal which overlaps with the resonance of the C2 proton of the imidazole ring such that only one broad line is observed (cross correlations #3, #4 with the alanyl-CH_2 protons are possible, but are too weak to cause a detectable line splitting). This signal contribution explains the higher intensity of H2 compared to H4.

Additional signals around $\delta = 7$ ppm can be caused by the connectivities #1 and #2, but the upfield shift relative to H4 indicates that only the coupling corresponding to ROE peak #1 is effective. An interaction referring to ROE peak #2 would require a restricted rotation around the C_β–$C_{imidazole}$ single bond while couplings within the rigid imidazole ring will always be strong. However, the connectivity of ROE peak #2 cannot be studied because the signal of the histidinyl-CH_2 protons, if detectable at all, would coincide in vivo with those of (P)Cr and Cho resonances. Although the observed asymmetric line positions point to a connectivity H2–H4 and although the rotation around the C_β–$C_{imidazole}$ single bond seems to be relatively unrestricted

Table 3
Negative cross peaks (ROE peaks) from HOHAHA experiments with intact frog gastrocnemius muscle studied by Alonso et al. [25]

	H2	H4	>NH	A, B	D	E
H2		1				
H4	1			2		
>NH					3	4
A, B		2				
D			3			
E			4			

>NH denotes the imidazole ring amino proton, other assignments according to Fig. 4.

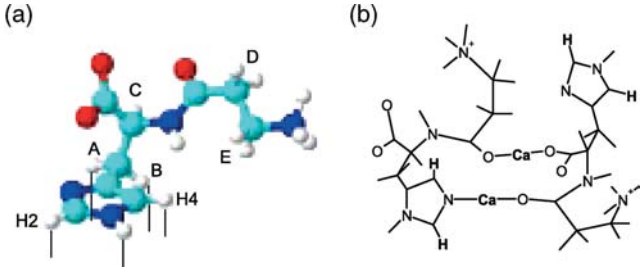

Fig. 9. (a) 3D structure of Cs in aqueous solution as proposed by Gaggelli et al. (adapted from Fig. 3 in [27]; labelling of protons, see Fig. 4). The imidazole ring is bent away from the chain structure which is also curved. Bars indicate the binding sites with bovine serum albumin according to [16]. (b) Sketch of the Dreiding model of the Ca^{2+} complex of carnosine in aqueous solution (adapted from Fig. 7 in [27]). H2 and H4 are indicated explicitly.

[16], molecular mobility with regard to binding of Cs to a macromolecular structure must also be discussed in general. This binding enables the mentioned connectivities by immobilizing specific groups of the molecule, but may also immobilize the entire molecule and thus counteract the averaging of dipolar couplings.

Studies of Cs binding to bovine serum albumin [16] or complex formation with Ca^{2+} [27] showed that the ring structure is bent away from the aliphatic structure as well as the histidinyl methylene group is twisted away (Fig. 9a). Binding to bovine serum albumin indicated H2, H4, A, and B as binding sites. The binding sites of Cs depend on the functional activity the molecule is involved in [16]. Our data suggest restricted motion mainly of the imidazole ring and possibly also of the peptide group; motional restrictions for protons A, B cannot be excluded, but seem to be less important.

Studies of Ca^{2+} complex formation of Cs in aqueous solution [27] demonstrated that two Cs molecules can be linked by two Ca^{2+} ions (Fig. 9b). For high concentrations [Ca^{2+}] (exceeding those in vivo), a very effective agglutination was observed enabling H2–H4 interaction. Since Cs presumably plays an important role in activation of Ca^{2+}-release channels and in subsequent muscle contraction [28], a specific binding of Cs is likely as well as the in vivo concentrations of this cation could enable the H2–H4 coupling. Even with extremely high values of [Ca^{2+}] not all Cs was bound to complexes [27]. Hence, a prevailing pool of mobile Cs will be present in tissue, in agreement with our observation of dominant signals of uncoupled spins.

Altogether, in living muscle tissue conditions exist that enable residual dipolar couplings between ^{1}H spins in Cs. The same effect has been demonstrated before for (P)Cr, Tau, and Lac. For Cs there are two additional aspects which support our interpretation of data.

First, the orientation dependency of Cs resonances in vivo [9] indicated the presence of residual dipolar couplings in this spin system. The effect can be observed for several metabolites in m. gastrocnemius but nearly vanishes in m. soleus for parallel alignment of the calf with B_0. According to Vermathen et al. [29,30], this can be explained by a different fibre orientation. The pennation angle θ is about 20° in m. gastrocnemius and 40°–50° in m. soleus for parallel alignment of the calf with the static magnetic field.

The joint appearance of additional lines of (P)Cr and Cs in one tissue and the absence or diminution of the effect in the other suggests the same physical explanation for the phenomenon in both metabolites.

Secondly, for the analysis of dipolar-coupling effects of spin systems at 1.5 T with small chemical-shift differences in the order of 1 ppm, second-order spectra must be considered. The observed asymmetries of in vivo ^{1}H NMR resonances in the Cs spectral region correspond to expectation. However, not all spectra could be fitted and the intensities and consequently the anticipated roof effect of X1–X4 could not be evaluated owing to the low S/N of these signals (Fig. 5) (the different signal modulation of X1–X4 complicates the line pattern additionally). Nevertheless, similar up- and downfield-shifts of the satellites were observed in all experiments confirming qualitatively the expected asymmetry parameters.

Since the asymmetries depend on the rotational angle α (Eq. (12)), they yield an alternative method to determine the dipolar coupling constant. The case that asymmetries can be observed at all demonstrates the difference of residual dipolar couplings of (P)Cr and Cs: the creatine methylene protons constitute an A_2 system and yield simple symmetric spectra as expected for the Paschen–Back regime, while Cs signals reflect an intermediate condition between the Zeeman and Paschen–Back regime.

At first sight, theory seems to treat isochronous spins inadequately as strongly coupled systems, since Eq. (5) permits the two cases $\Delta\omega = 0$ and $Sk \to \infty$. However, it is important to note that the Breit–Rabi diagram of Fig. 1b is not valid for isochronous spin systems: since $\Delta\omega = 0$, the rotation angle is fixed to $\alpha = 45°$ independent of the strength of the external field. Therefore, A_i systems are characterised by a simpler diagram showing only for the states 1 and 4 a linear dependency on the parameter x (details will not be discussed here). Thus the couplings of (P)Cr, Tau, and Lac can be described as "pseudo-strong" interactions and Cs is rather an AM system although the coupling constant is larger. These phenomena emphasize the effect of external fields on different systems of coupled magnetic moments not only in atomic physics but also for applications of NMR in vivo. It is interesting to note that the two Tau methylene groups yield just two doublets in in vivo ^{1}H NMR spectra corresponding to an A_2Z_2 system (for this spin system the scalar fine structure can be neglected in vivo) [2]. From the methylene positions in Tau dipolar couplings are expected not only within, but also between the groups. This connectivity should be relatively strong owing to the small chemical shift difference of 0.2 ppm. Hence, these four protons should rather constitute an A_2M_2 or at least an A_2X_2 system.

Breit and Rabi classified values $x < 0.1$ as weak field region [11] corresponding to a strong hyperfine interaction, which is not broken up by the external field. Because of the very small magnetic moments, nuclear spin couplings are compromised much easier (whereby protons form the most stable system because of the large γ) than interactions of nuclear-electronic systems. Additionally, the small difference of resonance frequencies for homonuclear systems causes the large slope of the two straight lines in Fig 1b. Hence, the upward energy shift of the two levels with $m_F = \pm 1$ relative to the other levels becomes less important when x increases. As

this shift is the origin of A_P, the transition from Zeeman to Paschen–Back regime occurs rapidly.

The only in vivo NMR signals known so far that exhibit resolved asymmetries because of transition from an AX to an AB system are the resonances of ATP in ^{31}P NMR spectra of muscle, liver, and brain and those of Cit in ^{1}H NMR spectra of the prostate (fine structures of other metabolite peaks, e.g., Tau and glutamate are usually not resolved in spectra of human tissue in vivo at 1.5 T). The interactions of these two systems differ not only qualitatively (involving J-couplings), but also quantitatively from that of Cs. The consequences of the rotation of the Hilbert subspace are less pronounced for ATP but significant for Cit.

The following points have to be considered for further studies of Cs resonances in vivo: Experiments which demonstrate the full orientation dependency would strengthen the argument that the line splitting is caused by dipolar coupling. Our examination of volunteers and of two muscle types with different pennation angles is one part to test the orientation dependency. The principal limitation originates from the acquisition times needed for sufficient spectral quality (about 15 min per spectrum), which are too long for the volunteers to keep the lower leg tilted and motionless for a whole series of measurements. Connectivities can possibly be detected in vivo by selective excitation of H4, subsequent observation of H2 and measurement of NOE signal enhancement. In addition, determination of the orientation dependence could clarify if transformation from the molecular to the magnet frame (by means of two Euler angles) is required. Studies of the (P)Cr methylene doublet in spectra from m. gastrocnemius showed that this is not the case because the Euler transformation was nearly an identity operation. Maximum line splitting was observed for nearly parallel orientation of the calf with respect to B_0 ($\theta \approx 0$), while the doublet collapses into a single line for a tilt of the lower leg by approximately 55° [1]. Analogous effects were reported for Cs [9] indicating that the fibre orientation of m. gastrocnemius closely matches the direction of the internuclear vector of the dipolar-coupled nuclei. Studies with Lac [3] were performed on excised hindlimb muscle; here the orientation was not predefined by the in vivo situation, however, the θ-dependent line splitting demonstrated that an Euler transformation into the molecule's frame had no significant effect.

Altogether, a residual dipolar coupling between C4- and C2-bound aromatic ring protons (H2 and H4) of histidine in the muscle peptide carnosine explains the NMR data obtained in our experiments. Now the coupling strength of this system can be estimated. Fig. 10 shows the observed line splittings Sk/h (Table 2) as a function of pennation angle θ (Table 1). Fit of these data with the function

$$Sk/h = SD_0(3\cos^2\theta - 1) \tag{17}$$

yields $SD_0 = (17.7 \pm 0.3)$ Hz (mean ± SD; neglecting corrections owing to Euler transformation). Hence the Breit–Rabi parameter for the strongest coupling ($\theta = 0°$) is $x = 3.60$ which is already very close to the Paschen–Back condition.

With the knowledge of this effective coupling constant, it is worthwhile to reconsider the Breit–Rabi diagram. Fig. 1 shows for $x > 0$ a crossing of two energy levels for dipolar-coupled spin systems. Level crossing (LC) spectroscopy was proposed in 1959 by Colegrove et al. [31] to study atomic fine structure and measure hyperfine structure constants. LC could also be relevant for dipolar-coupled protons as illustrated by the following: When the external magnetic field is adjusted such that two levels, say ψ_i and ψ_j cross, the corresponding transition will be quenched. Since x scales with Planck's constant, the field strength required to fulfil this condition is very small.

The first level crossing (descending from high x values) causes quenching of the transition $\psi'_2 \leftrightarrow \psi_1$ (Fig. 11). Consider the case of carnosine protons where $\Delta\omega \approx 1$ ppm. While E_2 is approximately $-0.5Sk$ for $x \ll 1$, the steep slope of E_1 as a function of x leads to LC at $x = 1.5 \times 10^{-6} = 2\hbar\Delta\omega/Sk$ which corresponds to an external field of 0.624 μT. Hence, in earth's magnetic field LC for dipolar-coupled protons of this mobility cannot be observed. However, recent progress in SQUID NMR spectroscopy demonstrates successful experiments in μT fields [32], making possible advanced studies of spin systems with residual dipolar couplings.

Low-field experiments are much more informative than those in high field for studying the aberration from

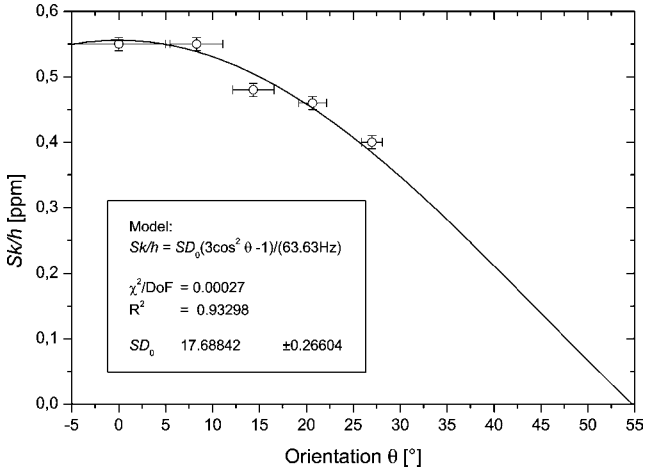

Fig. 10. Observed line splittings Sk/h of Cs resonances in m. gastrocnemius at different fibre orientations θ (measurement frequency: $\omega_0 = 63.63$ MHz). The accuracy of the measured (P)Cr-methylene line splittings is 0.7 Hz, resulting in varying errors at the different pennation angles. Fit with Eq. (17) supports the assumption of dipolar characteristics.

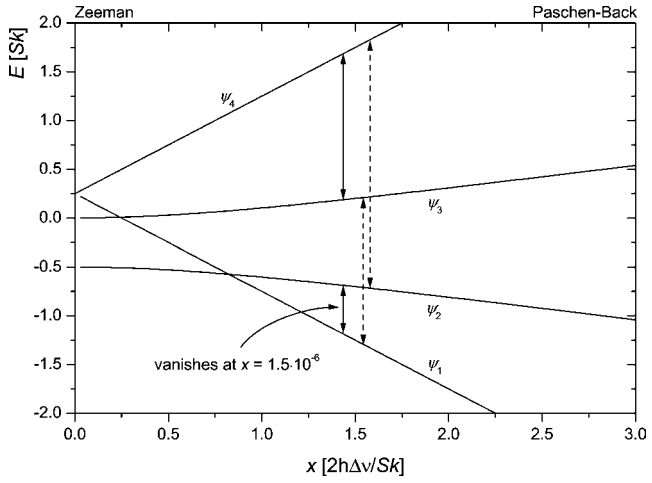

Fig. 11. Breit–Rabi diagram for dipolar-coupled protons illustrating the consequences of level crossing at very low fields. At $x = 1.5 \times 10^{-6}$ corresponding to $B_0 = 0.624\,\mu T$ the transition between the eigenstates 1 and 2 vanishes in the case of Cs. (The slope for the eigenstates 1 and 4 is scaled by the factor 0.5×10^{-6}.)

the normal Paschen–Back effect of weakly coupled systems. The actual progress in in vivo spectroscopy towards $B_0 \geqslant 3\,T$ enables experiments in the region of large x-values, thus masking these quantum mechanical effects.

Several questions concerning details of the Cs spectrum in vivo remain. For instance, it must be clarified what kind of binding causes the motional restriction of Cs molecules and influences one of the exchangeable NH protons. Specific binding to macromolecules or building-up of an electrical field within the myofilaments [33] which affects charged molecules has already been discussed in the context of Lac. Finally, for quantification particularly of (P)Cr in tissue it is important to know whether aliphatic resonances of Cs contribute to the in vivo spectrum.

Acknowledgment

The authors thank Christian Schmitz, M.Sc., for very valuable discussions about chemical aspects of Cs.

References

[1] R. Kreis, C. Boesch, Liquid-crystal-like structures of human muscle demonstrated by in vivo observation of direct coupling in localized proton magnetic resonance spectroscopy, J. Magn. Res. B 104 (1994) 189–192.

[2] H.J.A. in 't Zandt, D.W.J. Klomp, F. Oerlemans, B. Wieringa, C.W. Hilbers, A. Heerschap, Proton MR spectroscopy of wild-type and creatine kinase deficient mouse skeletal muscle: dipole–dipole coupling effects and post-mortem changes, Magn. Res. Med. 43 (2000) 517–524.

[3] I. Asllani, E. Shankland, T. Pratum, M. Kushmerick, Anisotropic orientation of lactate in skeletal muscle observed by dipolar coupling in ^{1}H NMR spectroscopy, J. Magn. Res. 139 (1999) 213–224.

[4] P.-G. de Gennes, J. Prost, The Physics of Liquid Crystals, second ed., Clarendon Press, Oxford, 1993.

[5] R. Kreis, M. Koster, M. Kamber, H. Hoppeler, C. Boesch, Peak assignment in localized ^{1}H MR spectra of human muscle based on oral creatine supplementation, Magn. Res. Med. 37 (1997) 159–163.

[6] H. Günther, NMR-Spektroskopie, Georg Thieme Verlag, Stuttgart, 1992.

[7] F. Schick, H. Bongers, S. Kurz, W.-I. Jung, M. Pfeffer, O. Lutz, Localized proton MR spectroscopy of the human prostate in vivo at 1.5 T, Magn. Res. Med. 29 (1993) 38–43.

[8] K. Straubinger, F. Schick, O. Lutz, Computer-algebra calculations and measurement on AB spin systems for double-spin-echo sequences, MAGMA 3 (1995) 109–118.

[9] R. Kreis, C. Boesch, Orientation dependence is the rule, not the exception in ^{1}H MR spectra of skeletal muscle: the case of carnosine, ISMRM Proc. 8 (2000) 31.

[10] L. Schröder, P. Bachert, Residual dipolar couplings in ^{1}H MR spectra of intact muscle in vivo reveal information about differences in molecular mobility of carnosine and creatine, MAGMA 15 (Suppl. 1) (2002) 270.

[11] G. Breit, I.I. Rabi, Measurement of nuclear spins, Phys. Rev. 31 (1931) 2082.

[12] R.K. Harris, Nuclear Magnetic Resonance Spectroscopy, Longman Scientific & Technical, Essex, 1986.

[13] K. Straubinger, F. Schick, O. Lutz, Influence of pulse angle variations on stimulated echo acquisition mode proton nuclear magnetic resonance spectra of AB spin systems: theory and experiments with citrate, MAGMA 7 (1998) 88–94.

[14] R.R. Ernst, G. Bodenhausen, A. Wokaun, Principles of Nuclear Magnetic Resonance in One and Two Dimensions, Clarendon Press, Oxford, 1997.

[15] C. Arús, M. Bárány, Application of high field ^{1}H NMR spectroscopy for the study of perfused amphibian and excised mammalian muscles, Biochim. Biophys. Acta 886 (1986) 411–424.

[16] C.E. Brown, F.L. Margolis, T.H. Williams, R.G. Pitcher, G.J. Elgar, Carnosine binding: characterization of steric and charge requirements for ligand recognition, Arch. Biochem. Biophys. 193 (1979) 529–542.

[17] H. Bruhn, J. Frahm, M.L. Gyngell, K.D. Merboldt, W. Hänicke, R. Sauter, Localized proton NMR spectroscopy using stimulated echoes: application to human skeletal muscle in vivo, Magn. Res. Med. 17 (1991) 82–94.

[18] J.W. Pan, J.R. Hamm, D.L. Rothman, R.G. Shulman, Intracellular pH in human skeletal muscle by ^{1}H NMR, Proc. Natl. Acad. Sci. USA 85 (1988) 7836–7839.

[19] R. Kreis, C. Boesch, Spatially localized, one- and two-dimensional NMR spectroscopy and in vivo application to human muscle, J. Magn. Res. B 113 (1996) 103–118.

[20] R.C. Harris, D.J. Marlin, M. Dunnett, D.H. Snow, E. Hultman, Muscle buffering capacity and dipeptide content in the thoroughbred horse, greyhound dog and man, Comp. Biochem. Physiol. A 97 (2) (1990) 249–251.

[21] C.L. Davey, The significance of carnosine and anserine in striated skeletal muscle, Arch. Biochem. Biophys. 89 (1960) 303–308.

[22] B.M. Damon, A.C. Hsu, H.J. Stark, M.J. Dawson, The carnosine C-2 proton's chemical shift reports intracellular pH in oxidative and glycolytic muscle fibers, Magn. Res. Med. 49 (2003) 233–240.

[23] V. Ntziachristos, R. Kreis, C. Boesch, B. Quistorff, Dipolar resonance frequency shifts in ^{1}H MR spectra of skeletal muscle: conformation in rats at 4.7 T in vivo and observation of changes post-mortem, Magn. Res. Med. 38 (1997) 33–39.

[24] J. Alonso, C. Arús, W.M. Wrestler, J.L. Markley, Two-dimensional correlated spectroscopy (COSY) of intact frog muscle: spectral pattern characterization and lactate quantitation, Magn. Res. Med. 11 (1989) 316–330.
[25] J. Alonso, C. Arús, W.M. Wrestler, J.L. Markley, Two-dimensional spectra of intact tissue: homonuclear Hartmann–Hahn spectroscopy provides increased sensitivity and information content as compared to COSY, Magn. Res. Med. 15 (1990) 142–151.
[26] V. Govindaraju, K. Young, A. Maudsley, Proton NMR chemical shifts and coupling constants for brain metabolites, NMR Biomed. 13 (2000) 129–153.
[27] E. Gaggelli, G. Valensin, ^{1}H and ^{13}C NMR relaxation investigation of the calcium complex of β-alanyl-L-histidine (carnosine) in aqueous solution, J. Chem. Soc. Perkin Trans. 2 (1990) 401–406.
[28] A.M. Rubtsov, Molecular mechanisms of regulation of the activity of sarcoplasmic Ca-release channels (ryanodine receptors), muscle fatigue, and Severin's phenomenon, Biochemistry (Moscow) 66 (10) (2001) 1132–1143.
[29] P. Vermathen, R. Kreis, C. Boesch, Mapping fiber orientation in human muscle by proton MR spectroscopic imaging, Magn. Res. Med. 49 (2003) 424–432.
[30] P. Vermathen, C. Boesch, S.E. Maier, R. Kreis, Comparison of fiber orientation in human muscle by short TE MRSI diffusion weighted imaging, ISMRM Proc. 10 (2002) 173.
[31] F.D. Colegrove, P.A. Franken, R.R. Lewis, R.H. Sands, Novel method of spectroscopy with applications to precision fine structure measurement, Phys. Rev. Lett. 3 (1959) 420–422.
[32] R. McDermott, A.H. Trabesinger, M. Mück, E.L. Hahn, A. Pines, J. Clarke, Liquid-state NMR and scalar couplings in microtesla magnetic fields, Science 295 (2002) 2247–2249.
[33] G.F. Elliott, C.R. Worthington, How muscle may contract, Biochim. Biophys. Acta 1200 (1994) 109–116.